



Automated sizing of permanent magnet synchronous machines with respect to electromagnetic and thermal aspects

Automated
sizing of PMSM

1205

Martin Hafner, Marc Schöning and Kay Hameyer

Institute of Electrical Machines, RWTH Aachen University, Aachen, Germany

Abstract

Purpose – The purpose of this paper is to consider thermal analysis as part of an automated sizing and design process. The temperature estimation at characteristic points of the machine, and in particular in permanent magnets, is essential to accurately simulate the electromagnetic behavior and avoid irreversible demagnetization.

Design/methodology/approach – In this paper, an electromagnetic dimensioning model, parameterized by finite element analysis, is coupled to a thermal lumped-parameter model to constitute a fast and efficient design tool for electrical machines.

Findings – A parameterized and hybrid FE-analytical electromagnetic model, which combines analytical and numerical advantages, to archive a fast and accurate electromagnetic simulation results is combined with a thermal lumped-parameter model for water-cooled and passive air-cooled surface mounted permanent magnet synchronous machines (PMSM).

Practical implications – Sizing, electromagnetic and thermal modeling aspects are integrated into an automated design process. The whole design process is demonstrated on two standard industrial servo motors for passive and active water cooling and afterwards compared with available measurements.

Originality/value – The proposed method allows considering thermal aspects during the iterative automated electromagnetic design process of PMSM.

Keywords Electric machines, Electromagnetism, Finite element analysis, Modelling, Temperature measurement

Paper type Research paper

1. Introduction

Especially, in case of high-power density permanent magnet synchronous machines (PMSM), the design process (Figure 1) is challenged by modeling the machine's internal thermal behavior. The temperature dependency of the permanent magnet remanence flux density strongly influences the results of the electromagnetic simulation. Moreover, even in worst case of the ambient temperature, winding and magnet temperature have to remain below their maximum temperature limit to prevent irreversible material damage. Therefore, thermal aspects have to be considered as an important part of the electromagnetic design process. Performing a thermal finite element analysis (FEA) for



The authors wish to express their gratitude to Bosch-Rexroth Group (Bosch Rexroth AG, 2010) who provided geometry and measurement data of the direct-drive MBT201D-0027. Moreover, the authors would like to gratefully acknowledge SEW-EURODRIVE (SEW-EURODRIVE, 2010) for providing a PMSM of the DS56L type series for measurement and the corresponding geometry data.

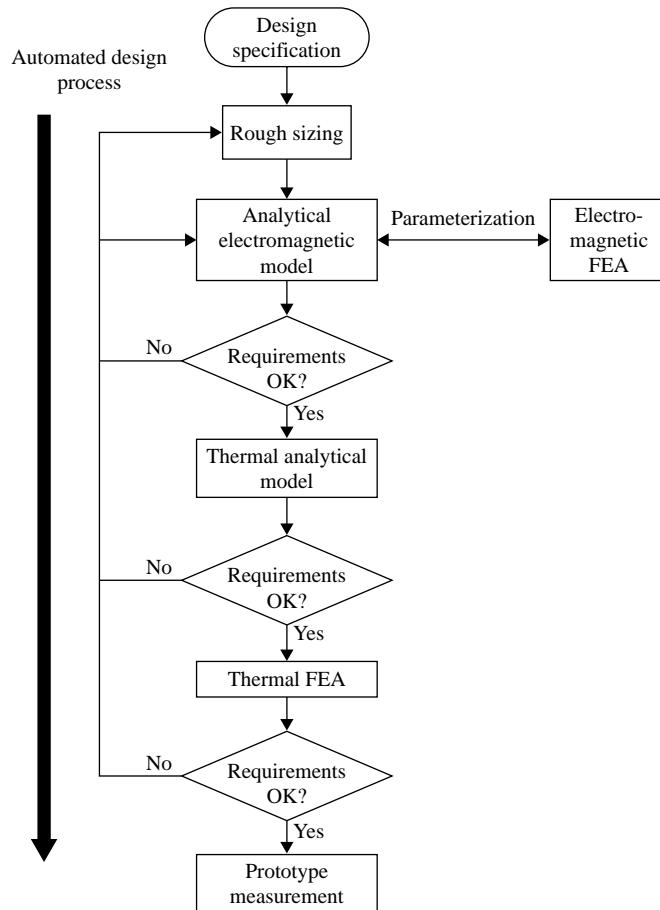


Figure 1.
Flowchart of automated
design process for PMSM

each design candidate of the machine is very time consuming and not acceptable at early design stages. In this paper, a lumped-parameter thermal model is coupled with the electromagnetic model presented in Schöning and Hameyer (2008b) to allow thermal analysis as part of an automated sizing and design process. Finally, the results of the coupled approach are compared with electrical and thermal measurements of two standard industrial servo-motors.

2. Automated design process

The software presented in this paper is specialized in the rapid-prototype development of electrical machines (Schöning and Hameyer, 2008a). Initially, a rough dimensioning on basis of classical design parameters such as rated torque, speed, and voltage is performed. Then a parameterized and hybrid FE-analytical electromagnetic model (Schöning and Hameyer, 2008b), which combines analytical and numerical advantages, is applied to achieve fast and accurate electromagnetic simulation results. The computed losses are automatically introduced as heat sources in the thermal model.

A post-processing layer monitors the deviation between results and predefined requirements after each calculation. If necessary, a feedback loop for optimization is initialized. Finally, the optimum machine design can be analyzed accurately by thermal FEA. The FEA is done with the iMOOSE package (van Riesen *et al.*, 2004; Schöning *et al.*, 2008), all other computations are based on Python (van Rossum, 2009) and the scientific Python extension (Oliphant, 2010).

3. Thermal analytical model

Lumped-parameter thermal models have shown to be effective in estimating the temperatures at critical locations in electrical machines. The approach is characterized by a short computation time and a good adaptability to empirical or knowledge-based data, although a minor loss of accuracy and detail can be observed in comparison to thermal FEA. This paper presents a modified version of the thermal lumped-parameter model presented in Lindström (1999), where a water-cooled surface mounted PMSM for a hybrid electric vehicle has been analyzed in steady-state and transient simulation assuming a constant reference temperature at the frame. The eight-node thermal equivalent circuit model of Lindström (1999) is shown in Figure 2. Each node represents a specific machine part. The thermal resistances between the nodes represent the motor's three-dimensional heat flow, considering material properties as well as the complex air gap and end winding convection behavior. The model has proved very

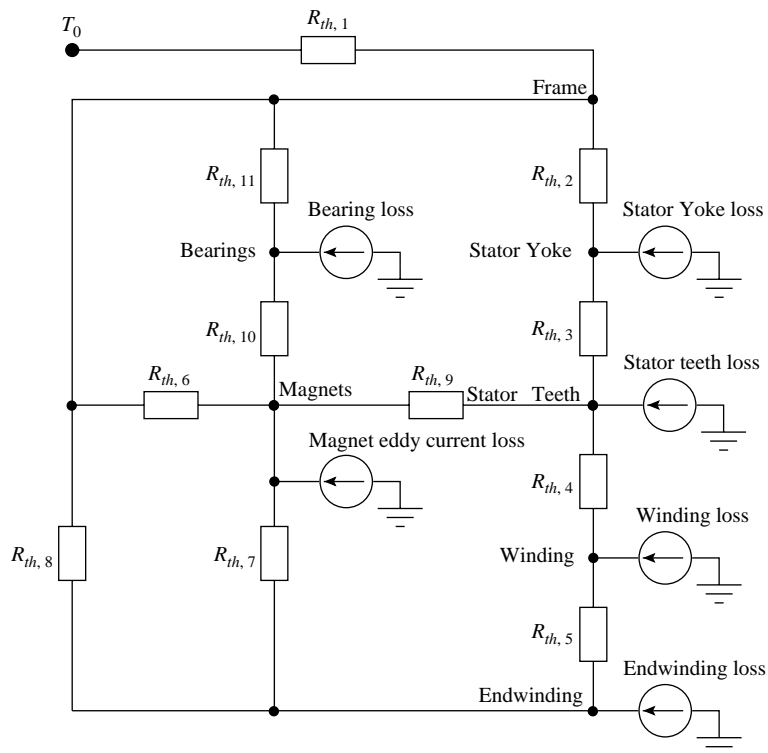


Figure 2. Thermal network model of a passive cooled surface mounted PMSM

flexible; EL-Refaie *et al.* (2004) presents an adaptation of this model for internal PMSM. Losses of electromagnetic origin, in stator teeth, stator yoke, and winding or end winding, are represented by equivalent currents injected into the network to determine the corresponding temperature rise (voltage) of each specific part with respect to T_0 . Lindström's simplification assuming an isothermal constant temperature around the frame (T_0) is replaced by modeling the heat transfer between frame and ambient air. In case of passive cooling, the frame temperature is a nonlinear function of the motor's radiation and convection properties. Before solving the network equations of Figure 2, the corresponding frame temperature T_0 has to be determined.

Newton's law, governing the heat convection, states:

$$Q_{con} = Ah(T_0 - T_\infty), \quad (1)$$

where Q_{con} is the power transferred by convection, A the involved frame surface, h an empirical convection coefficient, T_0 the average frame temperature and T_∞ the ambient air temperature. According to (VDI-Wärmeatlas, 2006) the heat transfer coefficient h around horizontally mounted cylinder can be estimated by:

$$h = \frac{Nu \cdot \lambda}{l} \quad (2)$$

$$= \frac{\lambda}{l} \{0.752 + 0.387 \sqrt[3]{Gr \cdot Pr \cdot f_3(Pr)}\} \quad (3)$$

$$Pr = \frac{\eta \cdot c_p}{\lambda} \quad (4)$$

$$Gr = \frac{g \cdot (T_0 - T_\infty) \cdot l^3}{T_\infty \nu^2} \quad (5)$$

$$f_3(Pr) = \left[1 + \left(\frac{0.559}{Pr} \right)^{9/16} \right]^{-16/9} \quad (6)$$

h depends on the characteristic length l , the thermal conductivity λ and the Nusselt number Nu , which is a function of Grashof number Gr and Prandtl number Pr . The effect of radiation is described by the Stefan-Boltzmann equation:

$$Q_{rad} = Ae\sigma (T_0^4 - T_\infty^4), \quad (7)$$

where Q_{rad} is the power transferred by radiation, e is the emissivity of the surface A , σ the Stefan-Boltzmann constant, T_0 the absolute temperature of the radiating frame and T_∞ the absolute ambient air temperature. According to equations (1) and (7) and the principle of energy-conservation, the governing equation for T_0 yields:

$$\sum_{i=1}^n Q_i = Q_{con} + Q_{rad} = A \left[e\sigma (T_0^4 - T_\infty^4) + h(T_0 - T_\infty) \right], \quad (8)$$

where Q_i denotes all heat sources within the machine. h itself is a nonlinear function of T_0 , (equation (3)), so that equation (8) needs to be solved iteratively.

4. Electromagnetic analytical model

Field of application of the analytical model is the design and recalculation process of PMSM. The purpose of the developed analytical model is the automated computation of various types of PMSM. Therefore, several types of constructions are considered. This includes the winding type, the slot shape and the magnets configuration. Distributed and concentrated windings, five different slot shapes as well as surface magnets or buried magnets are implemented. Owing to the absence of rotor windings and damper circuits, only the voltage equations and stator flux linkage have to be considered. In the rotating coordinate system, used to yield constant mutual reactances, the following set of steady-state equations is obtained (Vas, 1990):

$$V_d = R_1 \cdot I_d - X_q \cdot I_q, \quad (9)$$

$$V_q = R_1 \cdot I_q + X_d \cdot I_d + V_p, \quad (10)$$

$$T = \frac{3 \cdot p}{\omega} \cdot V_p \cdot I_q. \quad (11)$$

These are the main equations of the analytical model. The analytic iron loss computation is performed by the, Steinmetz like, formula:

$$p_{iron} = k \cdot B^\alpha, \quad (12)$$

where the coefficients k and α are determined by loss measurement of 1.0 and 1.5 T, generally provided by steel manufacturer for 50 Hz. On basis of the maximal air gap flux density B_δ^{max} the flux density of stator teeth B_{ts} and yoke B_y are estimated. The time-varying flux densities B_{ts} and B_y generate the following iron losses:

$$P_{teeth} = V_{ts} \cdot \rho \cdot p_{iron}(B_{ts}) \cdot \left(\frac{n \cdot p}{50 \text{ Hz}} \right)^{1.6} \quad (13)$$

$$P_{yoke} = V_y \cdot \rho \cdot p_{iron}(B_y) \cdot \left(\frac{n \cdot p}{50 \text{ Hz}} \right)^{1.6} \quad (14)$$

where V_{ts} and V_y are the volumes of the corresponding stator section, ρ the specific mass density of the laminated steel sheets, n the actual rotor speed and p the number of pole pairs.

5. Electromagnetic numerical simulation

The numerical simulation is performed using iMOOSE. This software package consists of solvers for different problem definitions such as static, transient, and harmonic problems. For all performed FE computations in this study, the node-based transient FEM solver for 2D electromagnetic field problems with eddy-current regions is employed. Owing to the requirements of an automated design process, the problem definition and the mesh must be generated automatically. The mesh generation is controlled by a Python-based scripting language, which transcribed a predefined machine model to common CAD file formats. To keep the modeling and meshing process flexible, they are parameterized through the output of the analytical model or directly by the geometrical data.

6. Validation

The presented design tool has been applied to two PMSM for industrial applications in order to validate the concept. In study Case A an industrial series PMSM is redesigned on basis of the rated performance data and the geometry specifications. The results are then critically compared to the real geometrical data. Afterwards, the results of the electromagnetic simulation and the thermal analysis are compared with measurements. Case B deals with a second shape optimized standard servo-drive, which requires designated modifications of the automated design process to demonstrate the flexibility of the electromagnetic and thermal model. Both study cases are electrical drives of actual series production, so that, in accordance with non-disclosure agreements, no geometry cross-sections or constructions details are given.

6.1 Study Case A

The first study case for validation is a PMSM of the DS56L type series produced by (SEW-EURODRIVE, 2010) (Figure 3a). The dimensioning process is initialized for a rated speed of 3,000 rpm and a rated torque of 2 N m, leading to 628 W rated power. Technical specifications imposed a concentrated winding with a phase voltage of



(a) PMSM of the DS56L type series produced by SEW-EURODRIVE



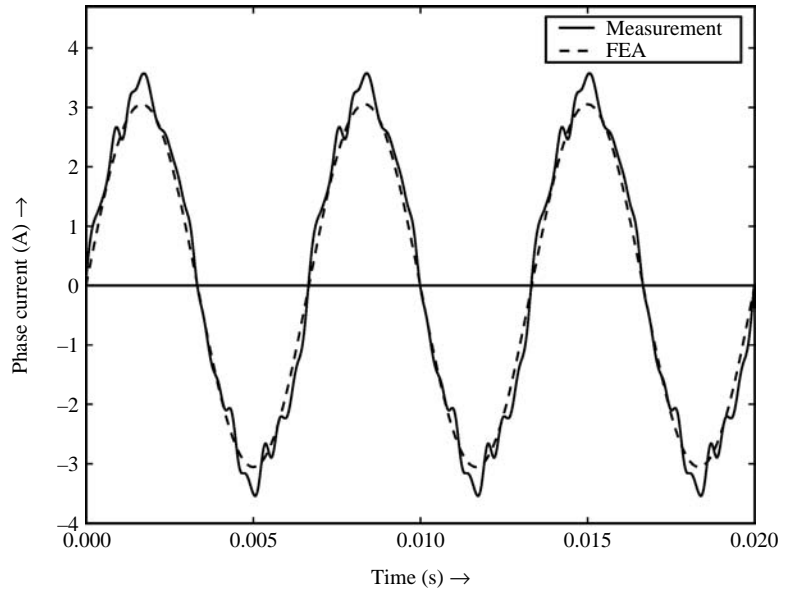
(b) MBT201D-0027 servo-drive, produced by the Bosch-Rexroth group

Figure 3.
Pictures of PMSM for industrial applications

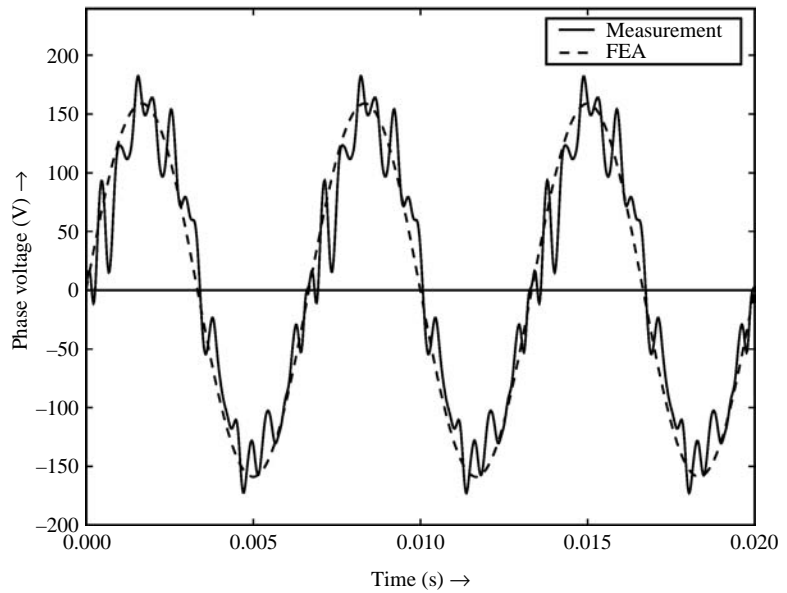
150/ $\sqrt{2}$ V. In accordance with construction-related designations, the stator slot shape is trapezoidal with rounded tooth tips. Moreover, magnet form and characteristic dimensions like, shaft diameter, copper fill factor, air gap height, and the ratio of inner stator diameter to active length are specified. On basis of these design parameters, the electrical and geometric dimensioning is performed according to the rules presented in Schönig and Hameyer (2008b). Table I lists the deviations between computed and actual cross-section characteristic length. The results of the sizing process are in good agreement with the actual dimension of the DS56L servo-drive; in order to verify the analytical and numerical methods, the virtual design process is continued with the original geometric dimensions of the DS56L. Assuming a sinusoidal current excitation, and using equation (11), the rated working point ($M = 2$ Nm, $n = 3,000$ rpm) is computed by analytic and numeric finite element simulation. In both cases, the phase voltage is determined by the electromagnetic steady-state equations (9) and (10). Figure 4(a) shows the measured phase currents in comparison with the assumed sinusoidal current. The corresponding phase voltage provided by measurement and FEA are shown in function of time in Figure 4(b). Both quantities, phase current and phase voltage, exhibit minor deviation with respect to measurements, which basically results from the assumption of a sinusoidal current excitation. The difference between analytic and numeric electromagnetic simulation is about 0.5 percent, so that an additional parameterization by FEA is not required, cf. Figure 1. The analytical model can be considered having an adequate efficiency, with respect to a FEA, for the computation of various working points. Table II compares the computed electric efficiency for the rated torque of 2 Nm in the speed range from 500 to 3,000 rpm with measurements. In terms of the presented application concept, a rapid-prototype development, these efficiency results are in good agreement. Figure 5 shows the machine's whole efficiency map, processed by Matplotlib (2010). In preparation for the thermal network model, iron losses in stator teeth and yoke are determined analytically by equations (13) and (14). Joule losses of the coil and the endwinding are identified by separating ohmic losses according to their proportion in volume. Bearing losses are estimated in function of the rotor speed, whereas eddy-current losses were neglected with respect to the machines power and speed. The DS56L is a servo-drive with natural convection, so that the average frame temperature T_0 is determined by solving equation (8) iteratively, with the nonlinear heat transfer coefficient h , defined by equations (2)-(6). The left-hand side of equation (8) is the sum of iron, joule and bearing losses. In case of an ambient air temperature of 23°C, the solution of equation (8) gives an average frame temperature of 77°C, which is in acceptable agreement with a measured frame temperature of 70°C. For the DS56L no further thermal measurements were available,

Geometry	Abs. deviation (mm)
Outer stator diameter	2.6
Stator yoke height	1
Stator tooth width	0.9
Stator tooth height	0.34
Tooth tip height	0

Table I.
Absolute deviation
between computed and
real cross-section profile
for relevant geometric
parameters in mm



(a) Phase current



(b) Phase voltage

Figure 4. Comparison between the measured and computed quantities phase voltage and phase current

so that the estimated temperature of the remaining nodes of the thermal lumped-parameter model could not be validated. The computational thermal results listed in Table III shows a common and characteristic temperature distribution within the machine parts, which indicate the effectiveness of the thermal model proposed.

Rotor speed (1/min)	Simulation (%)	Measurement (%)
500	60,77	61
1,000	74,66	72
1,500	80,7	80
2,000	84,02	82
2,500	86,07	86
3,000	87,44	88

Table II.
Efficiency in function of
the rotor speed for a
motor torque of 2Nm

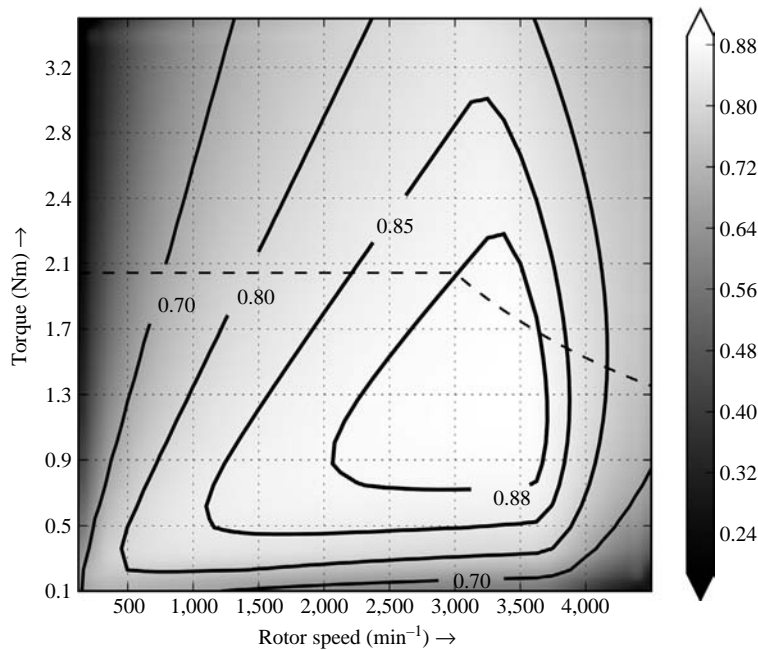


Figure 5.
Efficiency map of DS56L
for a power convert with
10 percent reserve voltage
capacity

Key temperature	Computation (°C)	Measurement (°C)
Frame	77	70
Stator yoke	76	
Stator teeth	79	
Coil	101	
Endwinding	110	
Magnet	80	
Bearing	78	

Table III.
Results of analytic
thermal equivalent
network computation of
DS56L for an ambient
temperature of 23°C

6.2 Study Case B

As a second example, the automated design process described in Section 2 has been applied to the MBT201D-0027 servo-drive, shown in Figure 3(b), a high-torque direct-drive motor of the IndraDyn T Series of the Bosch Rexroth Group (Bosch Rexroth AG, 2010). Catalog data sheet are given in Table IV. This servo-motor has a complicated and optimized geometry, so that the electromagnetic computation is performed numerically by a finite element computation. The whole design process, Figure 1, is conceived very flexible, so that particular computation blocks can be done analytically, numerically or in parallel to adapt them case by case. Iron losses are determined by a post-processing computation based on the modified Bertotti formula (Gracia *et al.*, 2007) and injected at the corresponding nodes of the thermal network. This machine has an active water-cooling system, so that the governing equation for the average frame temperature T_0 by passive heat transfer, equation (8), can be neglected. In normal operation, thermal measurement states an ingoing coolant temperature of 30°C and an outgoing cooling fluid temperature of 34°C. The temperature gradient of the frame along the z -direction can be represented by a mean temperature of 32°C, which is set as boundary condition for the node T_0 of the thermal equivalent network, cf. Figure 2. All thermal resistivities, except $R_{th,4}$, are computed by the provided geometry and material properties according to the general principles described in Lindström (1999). The lumped-parameter $R_{th,4}$ representing the thermal resistance between stator teeth and the inlaying coil wires, could not be determined analytically due to the uncommon stator shape of the motor. The thermal resistance $R_{th,4}$ has been varied, so that the simulated endwinding temperature complies with the experiment, see Table V. Without further modifications, the simulated and measured temperature in the magnets are identical, which indicates that the governing equations for the concentrated thermal resistances, representing complex machine parts, are reliable and applicable for standard

Table IV.
Data sheet of
MBT201D-0027

Rated value	Numerical value
Torque M_n	140 Nm
Speed n_n	330 min ⁻¹
Power P_n	4,84 kW
Voltage U_n	366 V
Current I_n	13 A

Table V.
Results of analytic
thermal equivalent
network computation of
MBT201D-0027 for an
average frame
temperature of 32°C

Key temperature	Computation (°C)	Measurement (°C)
Stator yoke	37	–
Stator teeth	67	–
Coil	114	–
Endwinding	131	130
Magnet	74	74
Bearing	80	–

geometries. Furthermore, the parameterization of $R_{th,4}$ exhibits, that empirical investigations or knowledge databases are important for thermal modeling.

7. Discussion

The proposed automated design process for PMSM, regarding electromagnetic and thermal aspects, see Figure 1, is implemented, by means of modern object-oriented programming, resulting in a flexible and multifunctional development process. The independent computation blocks, such as dimensioning, analytic and numeric electromagnetic model, thermal equivalent network, and numerical FEA, are combined sequentially by appropriate data structures. Iterations can be performed automatically or directly by a user interaction. If required, single blocks can be skipped, adapted, or modified. Necessary results in the subprocesses, required to complete the whole process, can be provided by equivalent types of computation, e.g. analytic or numeric situations, or the user itself. This proceeding is exemplified in study Case B, see Section 6.2, where the analytic electromagnetic simulation is directly replaced by FEA to analyze a geometry optimized servo-motor. Additionally, the geometric data has been specified, not determined by the sizing process. The results of the equivalent thermal network simulation are in agreement with measurements, and exhibit the characteristic temperature distribution. This demonstrates the practicability and flexibility of the applied analytic thermal model, but Case B shows some inherent limitations of this kind of approaches. For uncommon and complex geometry shapes classical analytic formula for individual thermal resistances are misleading, and resorting to empiric data or other feasible approaches, e.g. a parameterization by thermal FE method is required.

1215

8. Conclusions

The consideration of thermal phenomena is essential in the PMSM sizing process. Even if analytical thermal models estimate only the temperature at characteristic points of electrical machines and are not as detailed as whole FEA temperature distributions, it is worth seeking approximative models capable for rapid design processes. The presented approach extends the FEA parameterized electromagnetic dimensioning model of Schöning and Hameyer (2008b), with a thermal lumped-parameter model to consider thermal effects on the sizing process and the electromagnetic behavior. The whole design process is demonstrated with two standard industrial servo motors for passive and active water cooling. The redesign of one motor by the sizing process, on basis of classical design parameters, shows minimal deviations in the resulting geometric dimensions. Electromagnetic FEA results, performed for both test machines, are compared to the measured quantities phase voltage and phase current. In case of standard geometry, the utilized electromagnetic analytic model gains a sufficient accuracy with respect to measurement and FEA. Losses, obtained analytically, numerically or as combination of both, are injected as excitations in the automatically generated equivalent thermal network. Thermal measurements are compared with the estimation of the thermal model, showing its capability for standard geometries, but an inherent weakness for individual, nonstandard shapes. Further investigations are necessary to clarify which methods are appropriate to provide adequate data in that case and can be integrated into the design process. Moreover, the thermal equivalent model has shown to be very flexible and is also applicable to machines equipped with forced convection cooling systems (Hendershot and Miller, 1995).

References

- Bosch Rexroth AG (2010), available at: www.boschrexroth.com
- EL-Refaie, A., Harris, N., Jahns, T. and Rahman, K. (2004), "Thermal analysis of multibarrier interior PM synchronous machine using lumped parameter model", *IEEE Transactions on Energy Conversion*, Vol. 19 No. 2, pp. 303-9.
- Gracia, M.H., Lange, E. and Hameyer, K. (2007), "Numerical calculation of iron losses in electrical machines with a modified post-processing formula", *Proceedings of the 16th International Symposium on Electromagnetic Fields COMPUMAG, Aachen, Germany*.
- Hendershot, J.R. Jr and Miller, T.J.E. (1995), *Design of Brushless Permanent-Magnet Motors*, Oxford University Press, Oxford.
- Lindström, J. (1999), "Thermal model of a permanent-magnet motor for a hybrid electric vehicle", *Technical Report*, Department of Electric Power Engineering, Chalmers University of Technology, Göteborg.
- Matplotlib (2010), "A plotting library for the Python programming", available at: <http://matplotlib.sourceforge.net/>
- Oliphant, T. (2010), *Scientific Python (SciPy)*, available at: www.scipy.org/
- Schöning, M. and Hameyer, K. (2008a), "Applying virtual reality techniques to finite element solutions", *IEEE Transactions on Magnetics*, Vol. 44 No. 6, pp. 1422-5.
- Schöning, M. and Hameyer, K. (2008b), "Coupling of analytical and numerical methods for the electromagnetic simulation of permanent magnet synchronous machines", *COMPEL: The International Journal for Computation and Mathematics in Electrical and Electronic Engineering*, Vol. 27 No. 1, pp. 85-94.
- Schöning, M., Lange, E. and Hameyer, K. (2008), "Development and validation of a fast thermal finite element solver", *18th International Conference on Electrical Machines (ICEM 2008), Vilamoura*, pp. 1-5.
- SEW-EURODRIVE (2010), available at: www.sew-eurodrive.de
- van Riesen, D., Monzel, C., Kaehler, C., Schlensok, C. and Henneberger, G. (2004), "iMOOSE-an open-source environment for finite-element calculations", *IEEE Transactions on Magnetics*, Vol. 40 No. 2, pp. 1390-3.
- van Rossum, G. (2009), "Python programming language", available at: www.python.org
- Vas, P. (1990), *Vector Control of AC Machines*, Oxford University Press, Oxford.
- VDI-Wärmeatlas (2006), *VDI-Gesellschaft Verfahrenstechnik und Chemieingenieurwesen*, 10th revised ed. Springer, Berlin.

About the authors

Martin Hafner graduated in Electrical Engineering in 2006 at the RWTH Aachen University, Germany. His master thesis concerned the application of an energy-based vector hysteresis model to time harmonic FEA. Since 2007, he is working as a Research Associate in the Institute of Electrical Machines in Aachen, Germany. His research interests include the design and analysis of PMSM, hybrid FE-analytical electromagnetic machine models for rapid prototyping, and scientific visualization in virtual reality. VDE member. Martin Hafner is the corresponding author and can be contacted at: martin.hafner@iem.rwth-aachen.de

Marc Schöning received his MSc in 2004 and his PhD degree in 2009 from RWTH Aachen University. Since 2009, he is working as a Director of Research and Development for e + a, Elektromaschinen und Antriebe, in Switzerland. His fields of interest are virtual reality techniques as well as the development of analytical and numerical design tools for electrical machines.

Kay Hameyer was born in Hannover, Germany, on June 20, 1958. He received his MSc degree in Electrical Engineering from the University of Hannover and his PhD degree from the Berlin University of Technology. After his university studies, he worked with the Robert Bosch GmbH in Stuttgart as a design engineer for permanent magnet servo motors and board net components. Until 2004, Kay Hameyer was a full Professor for Numerical Field Computations and Electrical Machines with the KU Leuven in Belgium. Currently, he is the Director of the IEM and holder of the Chair Electromagnetic Energy Conversion of the RWTH Aachen University in Germany. VDE, IEEE senior member.